USGS
science for a changing world

# Marine Magnetic Survey and Onshore Gravity and Magnetic Survey, San Pablo Bay, Northern California

By David A. Ponce, Kevin M. Denton, and Janet T. Watt

Open-File Report 2016–1150

**U.S. Department of the Interior**
**U.S. Geological Survey**

**Cover—**Photograph of San Pablo Bay, California. View southeast across San Pablo Bay toward Carquinez Bridge. Photograph by D.A. Ponce, U.S. Geological Survey.

USGS
science for a changing world

# Marine Magnetic Survey and Onshore Gravity and Magnetic Survey, San Pablo Bay, Northern California

By David A. Ponce, Kevin M. Denton, and Janet T. Watt

Open-File Report 2016–1150

**U.S. Department of the Interior**
**U.S. Geological Survey**

**U.S. Department of the Interior**
SALLY JEWELL, Secretary

**U.S. Geological Survey**
Suzette M. Kimball, Director

U.S. Geological Survey, Reston, Virginia: 2016



Suggested citation:
Ponce, D.A., Denton, K.M., and Watt, J.T., 2016, Marine magnetic survey and onshore gravity and magnetic survey, San Pablo Bay, northern California: U.S. Geological Survey Open-File Report 2016–1150, 14 p., http://dx.doi.org/10.3133/ofr20161150.

ISSN 2331-1258 (online)

# Contents



## Figures



## Tables

## Conversion Factors

International System of Units to Inch/Pound

| Multiply | By | To obtain |
|---|---|---|
| | Length | |
| meter (m) | 3.28084 | foot (ft) |
| kilometer (km) | 0.6213 | mile (mi) |
| | Acceleration | |
| milligal (mGal) | $10^{-5}$ | meter per second squared ($m/s^2$) |

## Datum

Magnetic data are referenced to the horizontal North American Datum of 1983 (NAD83). Gravity data are referenced to the horizontal North American Datum of 1927 (NAD27) and the National Geodetic Vertical Datum of 1929 (NGVD29).

# Marine Magnetic Survey and Onshore Gravity and Magnetic Survey, San Pablo Bay, Northern California

By David A. Ponce, Kevin M. Denton, and Janet T. Watt

## Introduction

From November 2011 to August 2015, the U.S. Geological Survey (USGS) collected more than 1,000 line-kilometers (length of lines surveyed in kilometers) of marine magnetic data on San Pablo Bay, 98 onshore gravity stations, and over 27 line-kilometers of ground magnetic data in northern California (fig. 1). Combined magnetic and gravity investigations were undertaken to study subsurface geologic structures as an aid in understanding the geologic framework and earthquake hazard potential in the San Francisco Bay Area. Furthermore, marine magnetic data illuminate local subsurface geologic features in the shallow crust beneath San Pablo Bay where geologic exposure is absent.

Magnetic and gravity methods, which reflect contrasting physical properties of the subsurface, are ideal for studying San Pablo Bay. Exposed rock units surrounding San Pablo Bay consist mainly of Jurassic Coast Range ophiolite, Great Valley sequence (GVS), Franciscan Complex rocks, Miocene sedimentary rocks, and unconsolidated alluvium (Graymer and others, 2006). The contrasting magnetic and density properties of these rocks enable us to map their subsurface extent.

## Magnetic Data

### Marine Magnetic Data

Over 1,000 line-kilometers (length of lines surveyed, in kilometers) of marine magnetometer data were collected along approximately northeast- and northwest-trending traverses shown in figure 1. Shiptrack lines were spaced 200 meters (m) apart in a N. 55° E. direction, and tie lines were spaced 500 and 1,000 m apart in a N. 145° E. direction. Magnetometer and Global Positioning System (GPS) data were collected simultaneously at 1-second intervals using a Geometrics G858 cesium vapor magnetometer attached to a wooden pole extended about 2 m in front of the bow. The height of the magnetometer above the water surface was about 1 m. A portable Geometrics G856 proton-precession base-station magnetometer was used to record diurnal variations of the Earth's magnetic field during the marine magnetometer surveys and was installed near Point San Pablo for part of the survey and the Vallejo Marina for the remaining part of the survey.

Two vessels were used during the magnetic survey: a 32-foot sport fishing boat called the *Fury* and the 26-foot Radon USGS R/V *San Lorenzo*. The two vessels and the magnetic-survey system on the R/V *San Lorenzo* are shown in figure 2. Data collected from the *Fury* are shown as black lines in figure 1, and data collected from the R/V *San Lorenzo* are shown as red lines in

figure 1. During field operations, marine magnetic data were recorded and viewed in real time using Geometrics MagLog software. Raw magnetic data were downloaded and processed using Geometrics MagMap2000 software, where magnetometer and GPS data were merged. The location of the magnetometer system was recorded using a Trimble nonmagnetic Ag132 GPS receiver mounted on an aluminum frame attached to the cabin of the boat. The Ag132 receiver has real-time differential correction capabilities using an Omnistar satellite system, resulting in submeter horizontal accuracy. The data were collected in geographic coordinates (NAD83), and magnetic field values are expressed in nanoteslas (nT). Marine data were corrected for diurnal variations, filtered to remove cultural noise, leveled, and corrected for heading effects caused by the boat's magnetic field.

The local base-station data were compared to the Fresno Magnetic Observatory records obtained from the International Real-Time Magnetic Observatory Network (INTERMAGNET) (Kerridge, 2001) before removing the diurnal variations from the survey data. In addition, an International Geomagnetic Reference Field (IGRF) (for example, Finlay and others, 2010) was removed from the data.

A heading correction was applied to the marine magnetic data to account for the systematic shift in the magnetic readings owing to the magnetic field produced by the boat and its orientation. The heading correction was determined by piloting the boat over the same point while traveling in the direction of the survey lines: 55º, 145º, 235º, and 325º. The difference between the average value at the intersection point and the measured value for each direction is the heading correction. Magnetic readings that were not collected in the directions of the main survey lines (for example, turns) were removed from the survey.

After applying the heading correction, the difference in magnetic anomaly values where two survey lines cross was calculated for the southern magnetic survey (fig 1). Of 958 crossings, approximately 95 percent were below 5 nT, indicating that the marine magnetic readings are repeatable and have small crossing errors. The crossing values that were above 5 nT were from areas of high magnetic gradients where small GPS location differences result in greater crossing mismatches. The southern magnetic survey data were also low-pass filtered with a wavelength cutoff of 50 m that was applied to smooth high-frequency noise (~2 nT) caused by the movement of the boat on the water. The northern magnetic survey was datum shifted and joined with the southern magnetic survey, and data were gridded at a 50-m interval and shown as color-shaded relief maps in figures 3 and 4. The data are presented in table 1 as a comma delimited ASCII file. Although both survey lines (L) and tie lines (T) are included in the dataset, only survey lines were used to generate the grid and contour map (fig. 3).

## Ground Magnetic Data

Over 27 line-kilometers of ground magnetic data (fig. 1) were collected along the north shore of San Pablo Bay. Magnetometer and GPS data were collected simultaneously at 1-second intervals using a Geometrics G858 cesium vapor magnetometer and a Trimble GPS receiver mounted on a backpack with the sensor about 2 m above the ground. Ground magnetic data were corrected for diurnal variations of the Earth's magnetic field using a portable Geometrics G856 proton-precession base-station magnetometer, a regional IGRF (for example, Finlay and others, 2010) appropriate for the time of the survey, and single data spikes greater than 100 nT. The data are presented in table 2, and the format of all magnetic data is described in table 3. Geographic coordinates are in the NAD83 datum, and magnetic field values are in nanoteslas.

**Table 1.** Marine magnetic data.
[Table 1 is a comma delimited ASCII file and can be downloaded at https://pubs.er.usgs.gov/publication/ofr20161150]

**Table 2.** Ground magnetic data.
[Table 2 is a comma delimited ASCII file and can be downloaded at https://pubs.er.usgs.gov/publication/ofr20161150]

**Table 3.** Magnetic data format.

| Item | Symbol | Description | Comments, examples |
|---|---|---|---|
| 1 | LINE | Line number. L, survey line; T, tie line. | L0 |
| 2 | LAT | Latitude, in degrees. | NAD83 |
| 3 | LONG | Longitude, in degrees (west is negative). | NAD83 |
| 4 | TMA | Total magnetic anomly, in nanoteslas. | -65.73 |

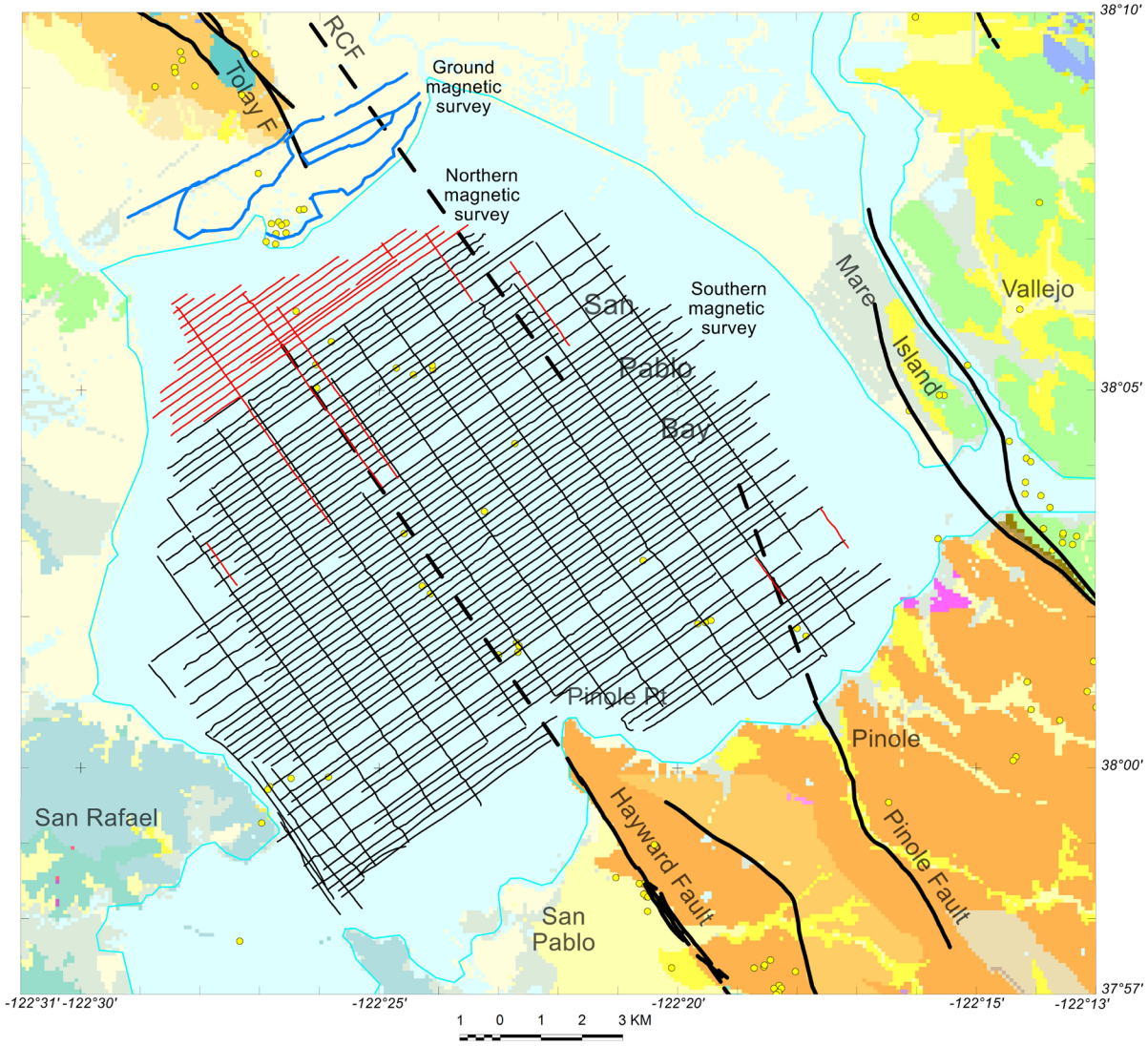


**Figure 1.** Index map of San Pablo Bay in northern California showing locations of marine and ground magnetic survey lines. Thin black lines, shiptracks from R/V *San Lorenzo* for southern part of marine survey; thin red lines, shiptracks from the *Fury* for northern part of marine survey; thick blue lines, ground magnetic lines. Geology: Black lines, faults; light yellows, Quaternary alluvium and mud deposits; tan, Miocene sedimentary rocks; forest green, Franciscan Complex rocks; lime green, Great Valley sequence (GVS) sedimentary rocks; purple, GVS volcanic rocks; yellow dots, seismicity data; RCF, Rodgers Creek Fault; Tolay F, Tolay Fault. Geology from Graymer and others (2006).


**Figure 2.** Marine magnetic system deployed on both the *Fury* and R/V *San Lorenzo*. A, The *Fury*. B, USGS R/V *San Lorenzo*. C, Magnetic sensor, located about 2 meters in front of the bow. D, Global Positioning System (GPS) antenna. Photographs by D.A. Ponce, U.S. Geological Survey.

## Gravity Data

Gravity data were collected at 98 locations along the north shore of San Pablo Bay (fig. 5) and concentrated in areas of poor control. Gravity data were processed using standard methods (Blakely, 1995) and included the following corrections: (1) an earth-tide correction, which corrects for tidal effects of the Moon and Sun; (2) an instrument-drift correction, which compensates for drift in the instrument's spring; (3) a latitude correction, which accounts for variation in the Earth's gravity with latitude; (4) free-air correction, which accounts for the variation in gravity owing to elevation relative to sea level; (5) a Bouguer correction, which corrects for the attraction of material between the station and sea level; (6) a curvature correction, which corrects the Bouguer correction for the effect of the Earth's curvature; (7) a terrain correction, which removes the effect of topography to a radial distance of 167 kilometers (km) from the station; and (8) an isostatic correction, which removes long-wavelength variations in the gravity field related to the compensation of topographic loads.

Scintrex CG-5 gravity meters were used in this study; the meter calibration was checked, and a secondary calibration factor was determined over the Mount Hamilton calibration loop (Barnes and others, 1969). Observed gravity values were based on a time-dependent linear drift between successive base readings and referenced to the International Gravity Standardization Net 1971 (IGSN 71) gravity datum (Morelli, 1974, p. 18). Free-air gravity anomalies were

calculated using the Geodetic Reference System 1967 formula for theoretical gravity on the ellipsoid (International Union of Geodesy and Geophysics, 1971, p. 60) and Swick's (1942, p. 65) formula for the free-air correction. Bouguer, curvature, and terrain corrections were added to the free-air anomaly to determine the complete Bouguer anomaly at a standard reduction density of 2,670 kilograms per cubic meter ($kg/m^3$). Finally, a regional isostatic gravity field was removed from the Bouguer field by assuming an Airy-Heiskanen model for isostatic compensation of topographic loads, with an assumed nominal sea-level crustal thickness of 25 km, a crustal density of 2,670 $kg/m^3$, and a density contrast across the base of the crust of 400 $kg/m^3$. Gravity values are expressed in milligal (mGal), a unit of acceleration or gravitational force per mass equal to $10^{-5}$ meters per second squared ($m/s^2$).

Station locations and elevations were obtained using a Trimble Geo7x differential GPS instrument. The Geo7x receiver uses the Wide Area Augmentation System, which in combination with a base station and postprocessing with a Continually Operated Reference Station (CORS), results in subdecimeter vertical accuracy. Locations are expressed in geographic coordinates using the NAD27 horizontal and NGVD29 vertical datums.

Terrain corrections, which account for the variation in topography near a gravity station, were calculated using a combination of manual and digital methods. Terrain corrections consisted of a three-part process: an innermost or field-terrain correction, an innerzone-terrain correction, and an outerzone-terrain correction. The innermost-terrain correction, which was estimated in the field, extends from the station to a radial distance of 68 m and is equivalent to the outer radius of Hayford and Bowie's (1912) zone B. The innerzone-terrain correction, which was estimated from a digital elevation model (DEM) with 10- or 30-m resolution derived from USGS 7.5-minute topographic maps, extends from 68 m to a radial distance of 2 km (D. Plouff, U.S. Geological Survey, unpub. data, 2006). The outerzone-terrain correction, which was calculated by using a DEM derived from USGS 1:250,000-scale topographic maps and an automated procedure based on geographic coordinates (Plouff, 1966, 1977; Godson and Plouff, 1988), extends from 2 km to a radial distance of 167 km. Digital terrain corrections were calculated by computing the gravity effect of each grid cell in the DEM, using the distance and difference in elevation of each grid cell from the gravity station.

Data from new gravity stations were combined with data from preexisting gravity stations (Langenheim and others, 2010). New data are listed in table 4, and the format is described in table 5. All gravity data were gridded using a minimum curvature algorithm at an interval of 500 m and displayed as a color-contoured isostatic gravity map (fig. 5). Observed gravity values are accurate to about 0.05 mGal, and calculated gravity anomalies are accurate to about 0.5 mGal.

**Table 4.** Gravity data.

[Table 4 is a comma delimited ASCII file and can be downloaded at https://pubs.er.usgs.gov/publication/ofr2016XXXX]

**Table 5.** Gravity data format and accuracy codes.

[mm, millimeter; cm, centimeter; m, meter; km, kilometer; in., inch; ft, foot; g/cm$^3$, grams per cubic centimeter; mGal, milligal; N.A., not applicable; IGSN71, International Gravity Standardization Net of 1971; NAD27, North American Datum of 1927; NGVD29, National Geodetic Vertical Datum of 1927; GPS, Global Positioning System; EDM, electromagnetic distance measurement; VABM, vertical angle bench mark]

| Item | Symbol | Description | Comments, examples | Null value |
|---|---|---|---|---|
| 1 | ID | Station name. | | N.A. |
| 2 | DATE | Date—year, month, and day (yyyymmdd). | 1974 to 75 | yyyymmdd |
| 3 | ACC | Four-digit accuracy code (8888=Discarded data). See Accuracy Codes. | | 9999 |
| 4 | LAT | Latitude, in degrees (south is negative). | NAD27 | 99.99999999 |
| 5 | LONG | Longitude, in degrees (west is negative). | NGVD29 | -999.99999999 |
| 6 | ELEV_M | Elevation, in m. | | 99999.999 |
| 7 | OG | Observed gravity, in mGal. | IGSN71 | 999999.999 |
| 8 | TG | Theoretical gravity, in mGal. | GRS67 | 999999.999 |
| GRAVITY CORRECTIONS | | | | |
| 9 | FAC | Free-air correction, in mGal. | Swick (1942) | 99999.999 |
| 10 | BC | Bouguer correction, in mGal. | | 99999.999 |
| 11 | CC | Curvature correction, in mGal (radius 166.7 km). | | 99999.999 |
| TERRAIN CORRECTIONS | | | | |
| 12 | FTC | Field terrain correction, in mGal. | | 99999.999 |
| 13 | R_FTC | Outer radius of FTC, in km (usually 0.068). | 0.068 | 99999.999 |
| 14 | ITC | Inner-zone terrain correction, in mGal. | | 99999.999 |
| 15 | R_RTC | Outer radius of ITC, in km (usually 2). If program Bouguer used, add 9000. | 2.000 | 99999.999 |
| 16 | OTC | Outer-zone terrain correction, in mGal (radius 166.7 km). | | 99999.999 |
| 17 | BTC | Bathymetric part of the terrain correction (radius 166.7 km). | | 99999.999 |
| 18 | FFTC | Far-field terrain correction from 166.7 km to 180 degrees, in mGal. | | 99999.999 |
| 19 | TTC | Total terrain correction, in mGal. | | 99999.999 |
| ISOSTATIC CORRECTIONS | | | | |
| 20 | ISOC | Isostatic correction, in mGal (radius 166.7 km). | | 99999.999 |
| 21 | FFISOC | Far-field isostatic correction from 166.7 km to 180 degrees, in mGal. | | 99999.999 |
| 22 | TISOC | Total isostatic correction (includes far-field isostatic and terrain corrections). | | 99999.999 |
| ANOMALIES | | | | |
| 23 | FAA | Free-air anomaly, in mGal. | | 99999.999 |
| 24 | SBA | Simple Bouguer anomaly, in mGal. | | 99999.999 |
| 25 | CBA | Complete Bouguer anomaly reduced for a density of 2.67 g/cm$^3$, in mGal. | | 99999.999 |
| 26 | ISO | Isostatic gravity anomaly reduced for a density of 2.67 g/cm$^3$, in mGal. | | 99999.999 |

| Code | Description | Meters | Feet | mGal |
|---|---|---|---|---|
| GENERAL LOCATION ACCURACY CODE | | | | |
| 1 | Ultra high-precision surveys (1 mm). For example, first-order level lines or theodolite surveys, GPS with long occupation times. | 0.001 | 0.002 | -- |
| 2 | High-precision surveys (2–3 cm). For example, using dual frequency GPS or EDM surveys. | 0.030 | 0.10 | -- |
| 3 | Surveys to 1/3 meter. For example, level-line benchmark. | 0.3 | 1 | -- |
| 4 | Surveys to 1 meter. | 1.0 | 3.3 | -- |
| 5 | Consumer GPS or other surveys. For example, transit or alidade surveys. | 3 | 10 | -- |
| 6 | "Spot" elevation or contour interpolation on 20-ft (6.1-m) contour map, good altimetry. | 10 | 20 | -- |
| 7 | Photogrammetry, other contour interpolation, poor altimetry. | 30 | 100 | -- |
| 8 | Bad station, discard, do not use. | -- | -- | -- |
| 9 | N.A. | -- | -- | -- |
| VERTICAL ACCURACY CODE | | | | |
| 1 | Millimeter. | 0.001 | 0.002 | 0.000 |
| 2 | 2–3 centimeters (0.1 ft). | 0.030 | 0.10 | 0.006 |
| 3 | 1/3-meter (1.0 ft). | 0.3 | 1 | 0.06 |
| 4 | Meter (for example, VABM). | 1.0 | 3.3 | 0.2 |
| 5 | Consumer GPS, spot elevation, or contour interpolation on 20-ft (6.1-m) contour map. | 3.0 | 10 | 0.6 |
| 6 | Consumer GPS, contour interpolation on 40-ft (12.2-m) contour map, good altimetry. | 6 | 20 | 1.2 |
| 7 | Contour interpolation on 80-ft (24.4-m) contour map. | 12 | 40 | 2.4 |
| 8 | Bad station, discard, do not use. | -- | -- | -- |
| 9 | N.A. | -- | -- | -- |
| HORIZONTAL ACCURACY CODE | | | | |
| 1 | 1/3-meter. | 0.30 | 1 | 0.000 |
| 2 | Meter. | 1.0 | 3.3 | 0.001 |
| 3 | Consumer GPS, spot elevation. | 3 | 10 | 0.002 |
| 4 | Location known to 0.01 in., on 1:24,000-scale map. | 6 | 20 | 0.005 |
| 5 | Triangulation or special survey. | 13 | 42 | 0.010 |
| 6 | Location known to 0.04 in., on 1:24,000-scale map. | 26 | 84 | 0.020 |
| 7 | 0.10 in., 1:24,000 or 0.04 in., 1:62,500-scale map. | 64 | 210 | 0.050 |
| 8 | Bad station, discard, do not use. | -- | -- | -- |
| 9 | N.A. | -- | -- | -- |
| OBSERVED GRAVITY ACCURACY CODE | | | | |
| 1 | Ultra-high-precision survey. | -- | -- | 0.001 |
| 2 | High-precision survey. | -- | -- | 0.01 |
| 3 | Multiple observations with LaCoste & Romberg or Scintrex meter. | -- | -- | 0.02 |
| 4 | Average LaCoste & Romberg or Scintrex gravity meter. | -- | -- | 0.05 |
| 5 | Average Worden meter. | -- | -- | 0.1 |
| 6 | Base closure error this large. | -- | -- | 0.5 |
| 7 | Base closure error this large. | -- | -- | 1.0 |
| 8 | Bad station, discard, do not use. | -- | -- | -- |
| 9 | N.A. | -- | -- | -- |

## Discussion

In general, magnetic anomalies reflect changes in the Earth's magnetic field and are typically used to infer lateral variations in the magnetization of rocks. Short-wavelength, high-amplitude magnetic anomalies are usually caused by volcanic rocks that are moderately to strongly magnetic. Long-wavelength or broad magnetic anomalies are often associated with large granitoid bodies.

Marine magnetic data (figs. 3 and 4) reveal a prominent magnetic anomaly immediately offshore of Pinole Point that probably reflects ultramafic rocks (for example, serpentinite), similar to those exposed in the northern part of the onshore Hayward Fault. Farther to the northwest, marine magnetic data enhance two prominent aeromagnetic anomalies along the Hayward Fault in the central part of San Pablo Bay. These magnetic anomalies appear to represent two separate features, one on either side of the Hayward Fault. Likely sources for these anomalies are probably mafic, ultramafic, or volcanic rocks along the fault. Indeed, the more prominent, higher amplitude anomaly, which occurs on the west side of the Hayward Fault, could reflect an offset counterpart to the San Leandro gabbro body in the central part of the onshore portion of the Hayward Fault (Ponce and others, 2003). If so, the apparent offset is about 43 km. A new strand of the Hayward Fault is imaged by shallow seismic reflection data (Watt and others, 2015) and can be seen as a subtle lineament in the magnetic data (fig. 3). Although a magnetic ridge of possible volcanic rock origin (Wright and Smith, 1992) occurs between the Hayward and Rodgers Creek Faults, the Rodgers Creek Fault itself is expressed by a gradient in the marine magnetic data. Analysis of these high-resolution marine magnetic data affords us the opportunity to image the detailed structure beneath San Pablo Bay and determine its implications for earthquake hazards.

Isostatic gravity anomalies in San Pablo Bay (fig. 5) primarily reflect lateral density variations in the middle to upper crust, and they can be used to infer the subsurface geology and structure. Gravity anomalies can reveal variations in lithology and features such as faults or deep sedimentary basins, which play a role in defining the geologic framework of San Pablo Bay.

Within San Pablo Bay, gravity-station control is poor because much of the area is covered by water and only a limited number of marine gravity stations are available. The gravity low in San Pablo Bay (fig. 5) reflects a moderately deep sedimentary basin filled with low-density alluvial, sedimentary, and volcanic deposits. Isostatic gravity data indicate the central part of San Pablo Bay corresponds to a 40-mGal gravity low. This yields a basin depth of about 3 km, assuming a density contrast of 0.4 grams per cubic centimeter ($g/cm^3$) between low-density deposits and bedrock, and using a semi-infinite slab approximation of the basin floor (for example, Nettleton, 1976; Blakely, 1995).

The physical property variations of the rocks that underlie this region are well suited to geophysical investigations. The contrast in density and magnetic properties between basement rocks and the overlying sedimentary and volcanic rocks and unconsolidated alluvium, for example, produces a distinctive pattern of gravity and magnetic anomalies. These anomalies can be used to infer subsurface geologic structure and aid in understanding the geologic framework of San Pablo Bay.

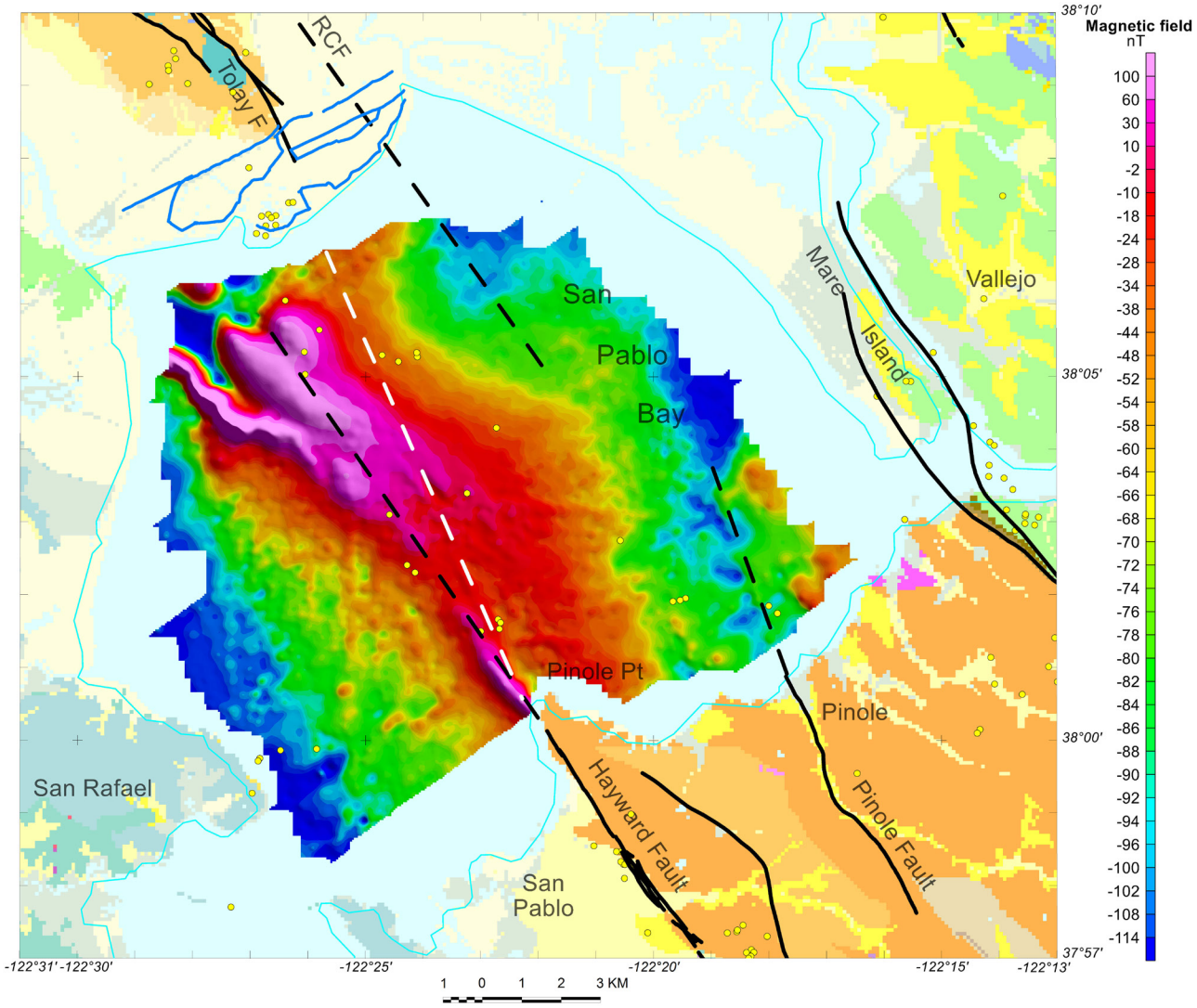


**Figure 3.** Marine magnetic map of San Pablo Bay, northern California. Prominent magnetic anomalies are associated with the Hayward Fault, and a magnetic lineament is associated with a new strand (white dashed line) of the Hayward Fault (Watt and others, 2015). RCF, Rodgers Creek Fault; Tolay F, Tolay Fault; nT, nanotesla.

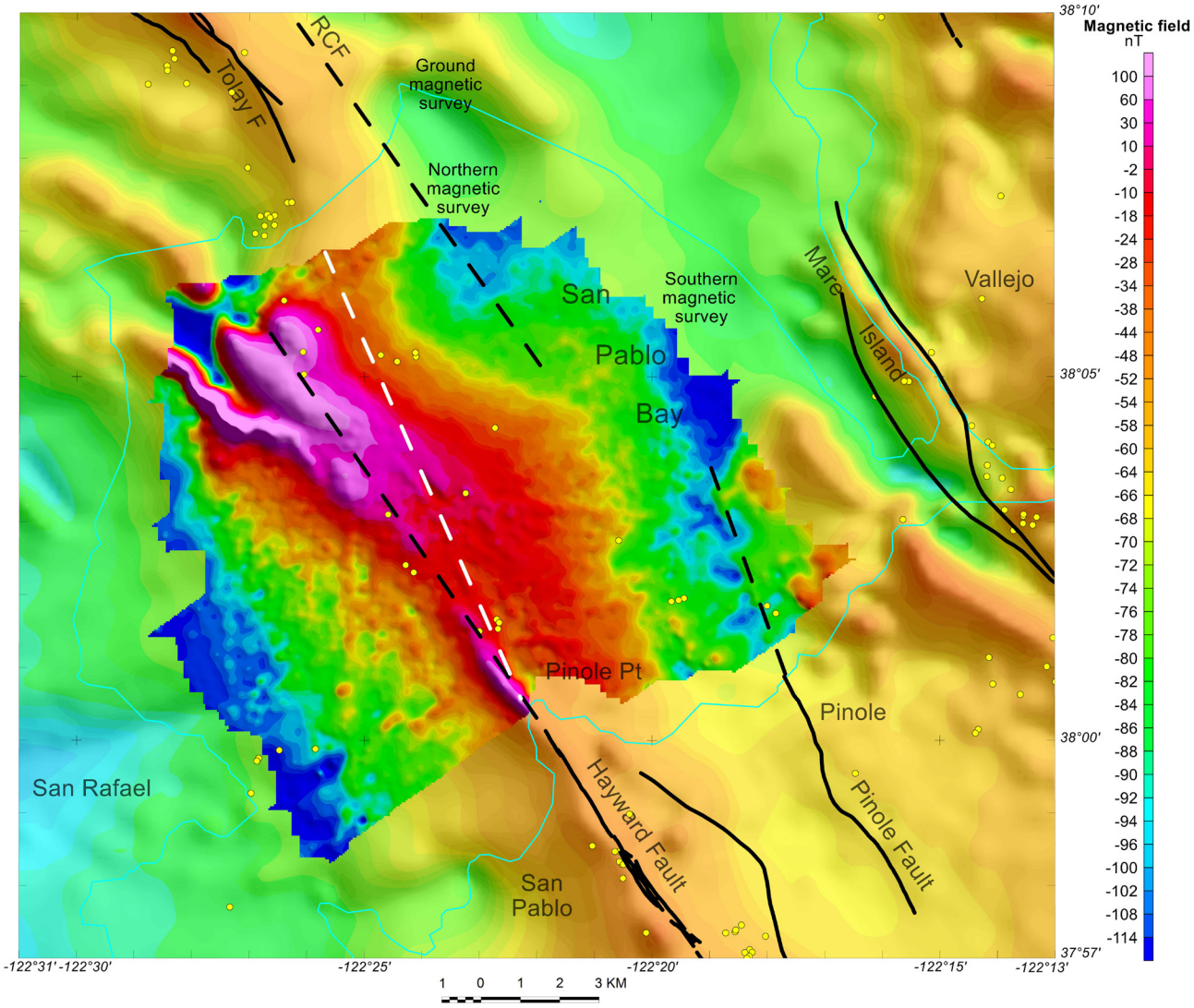


**Figure 4.** Marine magnetic map of San Pablo Bay, northern California, overlain on a regional aeromagnetic map (Roberts and Jachens, 1999). Black line, fault; cyan line, coastline. RCF, Rodgers Creek Fault; Tolay F, Tolay Fault; nT, nanotesla.

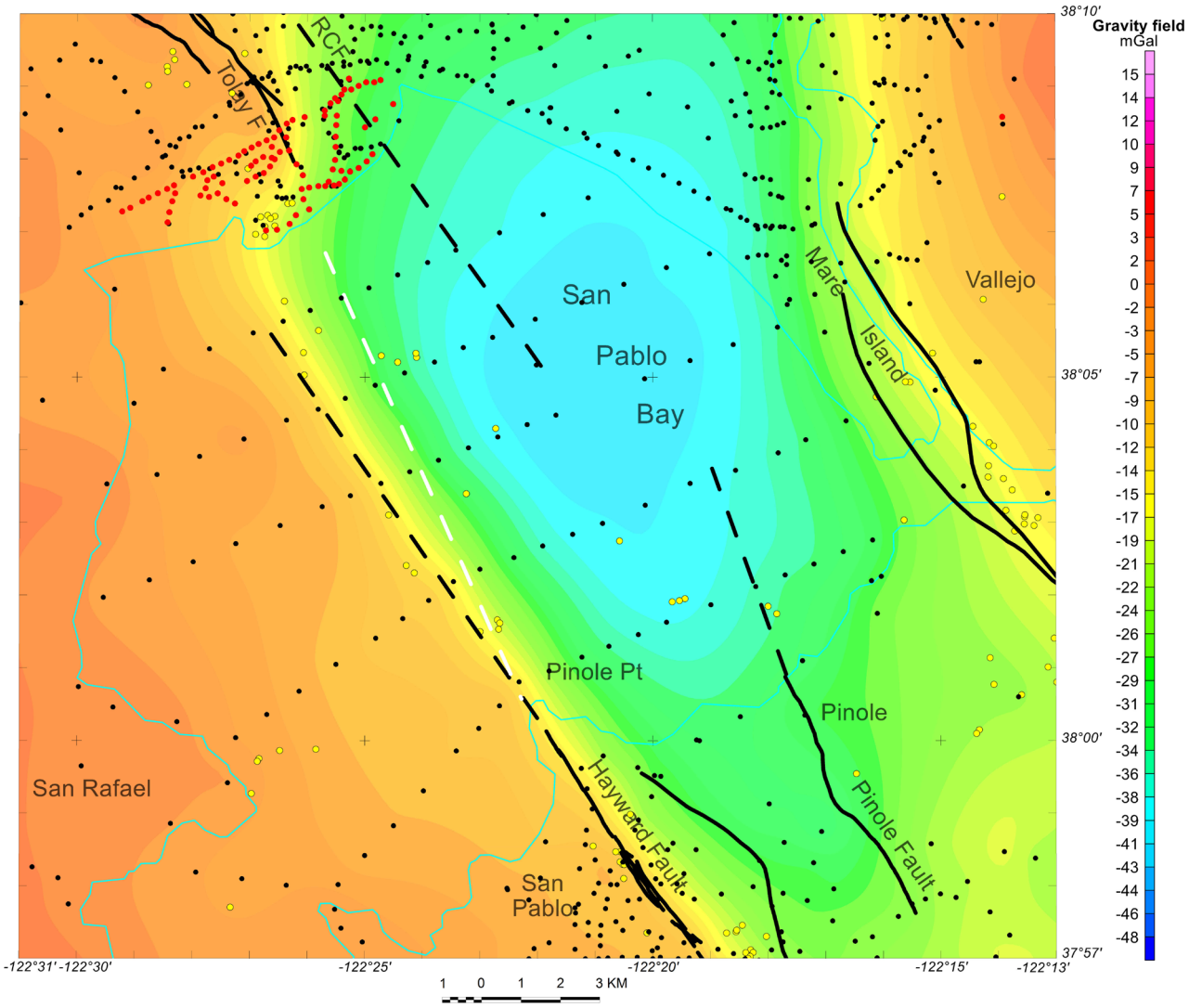


**Figure 5.** Isostatic gravity map of San Pablo Bay, northern California. Red dot, new gravity station located on the north shore of San Pablo Bay; black dot, previous gravity station; yellow dot, seismicity; black line, fault; cyan line, coastline. RCF, Rodgers Creek Fault; Tolay F, Tolay Fault; mGal, milligal.

## Acknowledgments

We thank Bruce Chuchel, Noah Athens, Carson MacPherson-Krutzsky, and Katherine Morgan of the USGS for field support and assisting in data processing. Diane Moore and Bruce Chuchel of the USGS provided helpful reviews and Jessica Dyke of the USGS edited the report. We extend special thanks to Captain Frank Miller of the *Fury* and Captain Jenny White of the USGS R/V *San Lorenzo* for their navigation and piloting skills in San Pablo Bay.

## References Cited

Barnes, D.F., Oliver, H.W., and Robbins, S.L., 1969, Standardization of gravimeter calibrations in the Geological Survey: Eos, American Geophysical Union Transactions, v. 50, no. 10, p. 626–627.

Blakely, R.J., 1995, Potential theory in gravity and magnetic applications: New York, Cambridge University Press, 441 p.

Finlay, C.C., Maus, S., Beggan, C.D., Bondar, T.N., Chambodut, A., Chernova, T.A., Chulliat, A., Golovkov, V.P., Hamilton, B., Hamoudi, M., Holme, R., Hulot, G., Kuang, W., Langlais, B., Lesur, V., Lowes, F.J., Lühr, H., Macmillan, S., Mandea, M., McLean, S., Manoj, C., Menvielle, M., Michaelis, I., Olsen, N., Rauberg, J., Rother, M., Sabaka, T.J., Tangborn, A., Tøffner-Clausen, L., Thébault, E., Thomson, A.W.P., Wardinski, I., Wei, Z. and Zvereva, T.I., 2010, International geomagnetic reference field—The eleventh generation: Geophysical Journal International, v. 183, p. 1216–1230.

Godson, R.H., and Plouff, D., 1988, BOUGUER version 1.0, a microcomputer gravity-terrain-correction program: U.S. Geological Survey Open-File Report 88–644–A, 22 p.

Graymer, R.W., Moring, B.C., Saucedo, G.J., Wentworth, C.M., Brabb, E.E., and Knudsen, K.L., 2006, Geologic map of the San Francisco Bay region, California: U.S. Geological Survey Scientific Investigations Map 2918, 1 pl., scale 1:275,000.

Hayford, J.F., and Bowie, W., 1912, The effect of topography and isostatic compensation upon the intensity of gravity: U.S. Coast and Geodetic Survey Special Publication 10, 132 p.

International Union of Geodesy and Geophysics, 1971, Geodetic reference system 1967: International Association of Geodesy Special Publication 3, 116 p.

Kerridge, David, 2001, INTERMAGNET—worldwide near-real-time geomagnetic observatory data: Workshop on Space Weather, European Space Research and Technology Centre, Noordwijk, The Netherlands, December 16–18, 2001, last accessed February 24, 2014, at http://nora.nerc.ac.uk/20521/, data available at http://www.intermagnet.org.

Langenheim, V.E., Roberts, C.W., McCabe, C.A., McPhee, D.K., Tilden, J.E., and Jachens, R.C., 2006, Preliminary isostatic gravity map of the Sonoma Volcanic Field and vicinity, Sonoma and Napa Counties, California: U.S. Geological Survey Open-File Report 2006–1056, scale 1:100,000.

Morelli, C., ed., 1974, The International Gravity Standardization Net 1971: International Association of Geodesy Special Publication 4, 194 p.

Nettleton, L.L., 1976, Gravity and magnetics in oil prospecting: New York, McGraw-Hill Book Company, 464 p.

Plouff, D., 1966, Digital terrain corrections based on geographic coordinates [abs.]: Geophysics, v. 31, no. 6, p. 1,208.

Plouff, D., 1977, Preliminary documentation for a FORTRAN program to compute gravity terrain corrections based on topography digitized on a geographic grid: U.S. Geological Survey Open-File Report 77–535, 45 p.

Ponce, D.A., Hildenbrand, T.G., and Jachens, R.C., 2003, Gravity and magnetic expression of the San Leandro gabbro with implications for the geometry and evolution of the Hayward fault zone, northern California: Bulletin of the Seismological Society of America, v. 93, no. 1, 11 p.

Roberts, C.W., and Jachens, R.C., 1999, Preliminary aeromagnetic anomaly map of California: U.S. Geological Survey Open-File Report 99–440, 14 p.

Swick, C.A., 1942, Pendulum gravity measurements and isostatic reductions: U.S. Coast and Geodetic Survey Special Publication 232, 82 p.

Watt, J.T., Ponce, D.A., Hart, P.E., Denton, K.M., Parsons, T., and Graymer, R.W., 2015, Detailed geophysical imaging in San Pablo Bay reveals a new strand of the Hayward-Rodgers Creek fault zone [abs.]: Eos, Transactions, American Geophysical Union, v. 95, no. 53.

Wright, T.L., and Smith, Neal, 1992, Right step from the Hayward fault to the Rodgers Creek fault beneath San Pablo Bay, *in* Borchardt, Glenn, Hirschfeld, S.E., Lienkaemper, J.J., McClellan, Patrick, Williams, P.L., and Wong, I.G., eds., Proceedings of the second conference on earthquake hazards in the eastern San Francisco Bay area: California Division of Mines and Geology Special Publication 113, p. 407–417.